

## Article

# Influence of Ag Doping on the Microstructural, Optical, and Electrical Properties of ZrSiN Coatings Deposited through Pulsed-DC Reactive Magnetron Sputtering

Henry Samir Vanegas Parra <sup>1,\*</sup>, Sebastián Calderón Velasco <sup>2</sup>, José Edgar Alfonso Orjuela <sup>3</sup> ,  
Jhon Jairo Olaya Florez <sup>4</sup> and Sandra Carvalho <sup>5</sup> 

<sup>1</sup> Grupo de Investigación Fundamental y Aplicada en Materiales (GIFAM), Departamento de Física, Universidad Antonio Nariño, Bogotá 111511, Colombia

<sup>2</sup> INL-International Iberian Nanotechnology Laboratory, Av. Mestre José Veiga s/n, 4715-330 Braga, Portugal; secave44@gmail.com

<sup>3</sup> Departamento de Física, Universidad Nacional de Colombia, Bogotá 111321, Colombia; jealfonsoo@unal.edu.co

<sup>4</sup> Departamento de Mecánica y Mecatrónica, Universidad Nacional de Colombia, Bogotá 111321, Colombia; jjolayaf@unal.edu.co

<sup>5</sup> SEG-CEMMPRE Department of Mechanical Engineering, University of Coimbra, 3030-788 Coimbra, Portugal; sandra.carvalho@dem.uc.pt

\* Correspondence: hsvanegas@uan.edu.co

**Abstract:** The functional properties of the transition-metal nitride coatings can be modified by adding noble metals such as silver. The incorporation of these elements has been demonstrated to be a good strategy for improving the electrical, optical, and mechanical responses of transition-metal nitride coatings. In this investigation, we report the production of Ag-ZrSiN coatings with varying silver atomic contents, deposited using pulsed-DC reactive magnetron sputtering. The effect of the incorporation of silver on the microstructure, the morphology, and the optical and electrical properties was investigated. The results revealed a nanocomposite structure of Ag-ZrSiN with nc-Ag/nc-ZrN embedded in an amorphous SiN<sub>x</sub> phase. The electrical resistivity decreased upon the incorporation of Ag from 77.99 Ω·cm to 0.71 Ω·cm for 0.0 and 12.0 at.% of Ag, respectively. A similar decreasing trend was observed in the transmittance spectra of the coatings as the silver content increased. For the Ag-ZrSiN coating, the transmittance values decreased within the wavelength range of 2500–630 nm and then remained constant down to 300 nm, at about 13.7%. Upon further increase of the silver concentration up to 12 at.%, the transmittance values continued to decrease between 2500 and 630 nm, reaching approximately zero at 630 nm, indicating that the coating becomes opaque within that spectral range.

**Keywords:** Ag-ZrSiN; sputtering; nanostructure



**Citation:** Vanegas Parra, H.S.; Calderón Velasco, S.; Alfonso Orjuela, J.E.; Olaya Florez, J.J.; Carvalho, S. Influence of Ag Doping on the Microstructural, Optical, and Electrical Properties of ZrSiN Coatings Deposited through Pulsed-DC Reactive Magnetron Sputtering. *Coatings* **2023**, *13*, 1154. <https://doi.org/10.3390/coatings13071154>

Academic Editor: Emmanuel Koudoumas

Received: 30 May 2023

Revised: 21 June 2023

Accepted: 25 June 2023

Published: 26 June 2023



**Copyright:** © 2023 by the authors. Licensee MDPI, Basel, Switzerland. This article is an open access article distributed under the terms and conditions of the Creative Commons Attribution (CC BY) license (<https://creativecommons.org/licenses/by/4.0/>).

## 1. Introduction

Nanostructured coatings of transition-metal nitride (TMN) have been utilized as protective coatings to enhance the durability of tools and mechanical components [1–18]. Among them, zirconium nitride (ZrN) has exhibited remarkable resistance to wear and corrosion, high hardness, excellent chemical stability, and biocompatibility [7,10,19–21]. Furthermore, ZrN coatings possess an appealing golden color, which has led to their application as decorative coatings [2,22]. In the past decade, several research groups have demonstrated that the physical and chemical properties of ZrN can be enhanced by the incorporation silicon (Si) as an additional element [7,14,17,23–27]. The inclusion of Si within the ZrN matrix can result in either a nanocomposite or a nanostructured coating, depending on the deposition technique and the parameters employed [28]. Basically, these coatings comprise two phases: nanocrystalline zirconium nitride and amorphous

silicon nitride ( $\text{Si}_3\text{N}_4$ ) [22,26,29]. Certain studies have highlighted the significance of the chemical composition and the thickness of the amorphous  $\text{Si}_3\text{N}_4$  phase concerning the optical and electrical properties of such coatings [30,31]. For instance,  $\text{Si}_3\text{N}_4$  has exhibited optical transparency across the ultraviolet to the infrared region and has exhibited electrically insulating properties [32]. Musil et al. [33] deposited Si-ZrN films by means of the sputtering technique and discovered that the films with a Si atomic content of 25 at.% or higher are amorphous, electrically insulating, and optically transparent. These coatings have been proposed as protective coatings on glass molding dies [7] due to their typically higher nanohardness values compared to those of common glass (3 to 7 GPa) [30,31].

In order to enhance the functional properties such as hardness of TMN-Si systems, various groups have proposed the incorporation of metallic nanoparticles such as silver. These works are summarized in Table 1 [5,34].

**Table 1.** Ceramic matrix with incorporation of silver.

Reference	Deposition Method	Coating
Domingues et al. [4]	DC reactive magnetron sputtering.	Ag-AlN Au-AlN Cu-AlN
Cavaleiro et al. [5,15]	High-power impulse magnetron sputtering.	Ag-TiSiN
Dang et al. [34]	Co-sputtering in a multi-arc ion plating system.	Ag-TiSiN
Popović et al. [35]	DC reactive sputtering.	TiN irradiated with Ag

Additionally, it has been demonstrated that metallic nanoparticles can introduce specific functionalities to coatings, such as a low-friction coefficient, hydrophobicity, antibacterial properties, and the surface plasmon resonance effect [4,36–38] (Table 1). Domingues et al. [4] deposited Ag-AlN thin films via DC magnetron sputtering, and the results showed a localized surface plasmon resonance at wavelengths around 380 nm when the films were annealed at 300 °C. According to the authors, the presence of Ag particles led to a nearly flat absorption band from visible to infrared wavelengths. Cavaleiro et al. [15] investigated the influence of silver on the tribological behavior of Ag-TiSiN coatings deposited via sputtering. Their study indicated that the silver had a positive effect on the wear resistance when the tribology test was conducted using  $\text{TiAl}_6\text{V}_4$  balls. Dang et al. [34] utilized co-sputtering in a multi-arc ion plating system to deposit a Ag-TiSiN nanocomposite. The authors reported that at a Ag atomic content of 1.4 at.%, the hardness reached 36.0 GPa. However, with an increase in the Ag content, the hardness decreased, due to the increase of the soft phase (Ag), while the wear resistance improved, due to Ag segregation to the surface of the coatings. Popović et al. [35], employing sputtering, prepared titanium nitride (TiN) films that were irradiated with Ag ions, and the results demonstrated the presence of surface plasmon resonance, attributed to silver particles. Furthermore, the incorporation of Ag affected the metallic behavior of TiN films. However, with the advancement of aerospace and solar technology, there is an increasing demand for optical coatings with a high durability, including high hardness, wear resistance and high corrosion resistance. Obtaining such optical coatings poses significant challenges [39]. Therefore, optical coatings with metal nanoparticles are of significant interest in various fields, including tribology [34] and optics [4], owing to their potential to enhance physical properties that depend on the microstructure and morphology [4,5,34]. In the present investigation, a novel nanostructured coating of Ag-ZrSiN was deposited by means of sputtering with different Ag atomic contents, and the influence of Ag incorporation on the microstructure, morphology, and electrical and optical properties was investigated in order to gain insight into how silver affects the physical properties of ZrSiN nanostructured coatings.

## 2. Materials and Methods

### 2.1. Coating Deposition

Ag-ZrSiN coatings with varying Ag atomic content were deposited by means of the pulsed-DC reactive magnetron sputtering technique in an Ar/N<sub>2</sub> atmosphere. For the analysis, different substrates, including glass, silicon, and stainless steel (316 L), were utilized, and these substrates were subjected to standard cleaning procedures before the deposition process [24].

The deposition chamber was equipped with a 50 mm diameter zirconium (Zr) target of 99.7% purity. Pellets of Si and Ag measuring  $3.0 \times 3.0 \text{ mm}^2$  were positioned on the erosion track of the target. Throughout the sputtering process, the working pressure was maintained at approximately 0.8 Pa, and a DC power of 140 W was applied to the Zr-Si-Ag target. The deposition time for all coatings was set at 60 min. The Ag content in the ZrSiN coatings was adjusted by varying the number of Ag pellets on the target surface, specifically 0, 1, or 2 pellets. Detailed experimental information is summarized in Table 2. Further information regarding the sputtering equipment used and other parameters can be found elsewhere [24].

**Table 2.** Details of experimental parameters used to deposit the Ag-ZrSiN coatings. The thickness was determined by cross-sectional SEM images.

Samples	Number of Pellets		Sputtering Parameters				
	Si	Ag	Base Pressure (Pa)	Work Pressure (Pa)	Power (W)	Sputtering Time (min)	Thickness (nm)
ZrSiN	1	0	$4 \times 10^{-4}$	0.8	140	60	$955 \pm 8$
1Ag-ZrSiN	1	1	$4 \times 10^{-4}$	0.8	140	60	$1115 \pm 4$
2Ag-ZrSiN	1	2	$4 \times 10^{-4}$	0.8	140	60	$1219 \pm 9$

### 2.2. Characterization of the Coatings

The surface and cross-sectional morphology of the coatings was examined using a NanoSEM—FEI Nova 200 FEG/SEM microscope operating in secondary electron (SE) mode, equipped with an energy-dispersive X-ray (EDS) system for the elemental composition analysis. X-ray photoelectron spectroscopy (XPS) was utilized to investigate the chemical binding energy in the coatings, employing a Kratos AXIS Ultra HAS. X-ray diffraction (XRD) analysis was performed in the  $\theta$ - $2\theta$  geometry from  $20^\circ$  to  $90^\circ$  in order to explore the crystalline structure. For a comprehensive investigation of the chemistry and the morphology, aberration-corrected (scanning) transmission electron microscopy (ac-(S)TEM) was employed, utilizing a double aberration-corrected FEI Titan Themis microscope operating at 300 keV. The frequency and particle size distribution of the coatings was determined by ImageJ software. The surface SEM images were first transformed into a grayscale map, and then a binary mask was applied to enable the quantification of the particles. The nanohardness was determined through nanoindentation using a Hysitron TI 750 Ubi instrument. Reflectance and transmittance measurements were carried out using UV-visible-NIR spectrophotometry across a wavelength range of 300 to 2500 nm. The electrical behavior was assessed at room temperature using the Van der Pauw method. Further details regarding the equipment used can be found in previous articles [24,31].

## 3. Results and Discussion

### 3.1. Elemental Composition of the Ag-ZrSiN Coatings

Table 3 presents the elemental composition of the deposited coatings. The results demonstrate that the incorporation of Ag pellets on the surface of the Zr target directly affects the Ag atomic content in the coatings, increasing twofold as the number of pellets are doubled. Moreover, as the Ag content increases, the atomic content of Zr and N decreases. The decrease in the Zr content is related to the reduction of the erosion zone of target, caused by the presence of Ag pellets [40]. On the other hand, the decrease in the N content is due

to the fact that Ag does not spontaneously form nitrides, as indicated by the high enthalpy of formation (+314 kJ/mol) between silver and nitrogen [41]. Conversely, the formation of ZrN and Si<sub>3</sub>N<sub>4</sub> is favorable, given the enthalpy of the respective reactions (−365.5 kJ/mol and −745.1 kJ/mol) [41]. However, it should be noted that Ag and a transition-metal nitride such as ZrN and Si<sub>3</sub>N<sub>4</sub> are immiscible [13,42]. Therefore, the presence of Si<sub>3</sub>N<sub>4</sub>, ZrN, and metallic Ag in the coatings is to be expected.

**Table 3.** EDS results of the Ag-ZrSiN coatings.

Coatings	Zr (at.%)	N (at.%)	Si (at.%)	Ag (at.%)	O (at.%)	(Zr + Si)/Ag
ZrSiN	43.0	49.0	8.0	0.0	0.0	-
1Ag-ZrSiN	39.0	47.0	8.0	6.0	0.0	7.8
2Ag-ZrSiN	36.0	41.0	7.0	12.0	4.0	3.6

### 3.2. Morphological and Microstructural Analysis of the Ag-ZrSiN Coatings

To investigate the impact of the incorporation of Ag into the ZrSiN matrix on the morphology and microstructure of the coatings, comprehensive characterizations were conducted, employing scanning electron microscopy (SEM), scanning transmission electron microscopy (STEM), and X-ray diffraction (XRD). Figure 1 displays a cross-section of ZrSiN and Ag-ZrSiN coatings with varying Ag content, while Figure 2 presents the top-view images of the coatings.

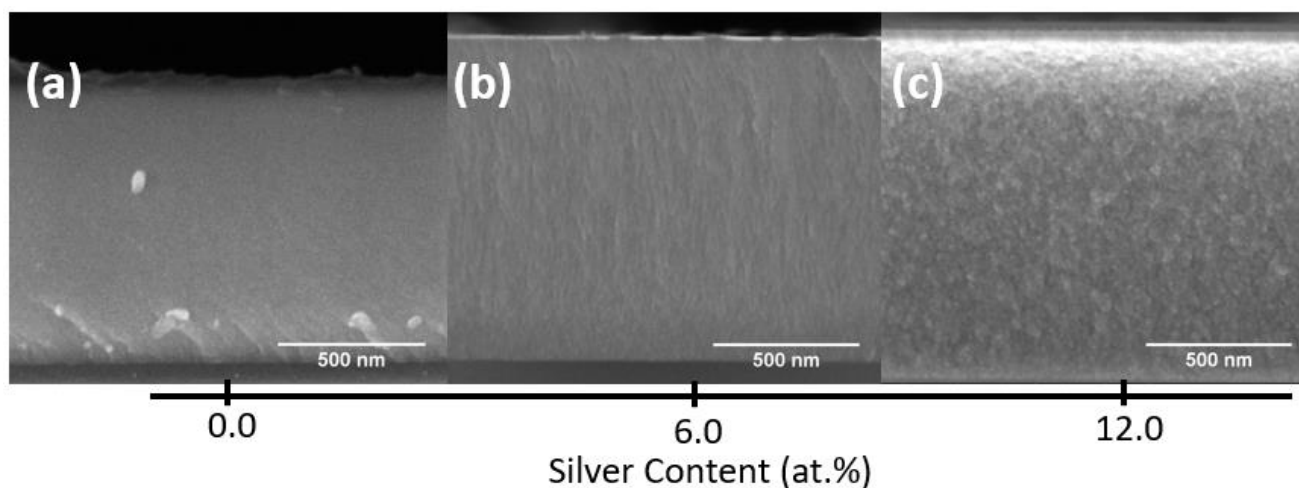


**Figure 1.** Cross-sectional SEM micrographs of the (a) ZrSiN, (b) 1Ag-ZrSiN, and (c) 2Ag-ZrSiN coatings.

Figure 1a illustrates the cross-sectional morphology of the ZrSiN coating, displaying a homogeneous and featureless morphology. Upon the introduction of Ag, the cross-sectional morphology of the coatings undergoes noticeable changes. Figure 1b depicts the Ag-ZrSiN coating with a silver content of 6 at.%, revealing a fine nano-columnar growth pattern. By contrast, Figure 1c exhibits the coatings with 12 at.% Ag, characterized by a granular morphology, with the presence of nanosized particles.

To verify the presence of Ag particles on the samples' surface, SEM micrographs of the top surface were captured, as presented in Figure 2. Figure 2a illustrates the surface morphology of the ZrSiN coating, exhibiting a homogeneous appearance without the presence of particles, pores, or grains. This observation is consistent with the cross-sectional analysis, where no columns were observed in the coating. However, upon the incorporation of Ag, as shown in Figure 2b, particles were uniformly dispersed on the surface, with an average diameter of  $12.6 \pm 5.4$  nm. As the silver content in the coatings increases, as depicted in Figure 2c, an increase in surface segregation can be observed, with the Ag particle exhibiting a diameter of  $15.6 \pm 6.2$  nm. According to previous studies [13,34,43,44], the presence of these particles on the surface corresponds to metallic Ag. During the deposition

process, the Ag particles undergo segregation to the intercolumnar spaces of the ZrSiN or become embedded within the amorphous phase of SiN<sub>x</sub>, owing to the immiscibility between the Ag and the ceramic matrix. Furthermore, the elevated temperature employed during the deposition process promotes the diffusion of Ag particles to the coatings' surface, leading to their growth and agglomeration and the formation of silver nanoparticles on the surface [45].

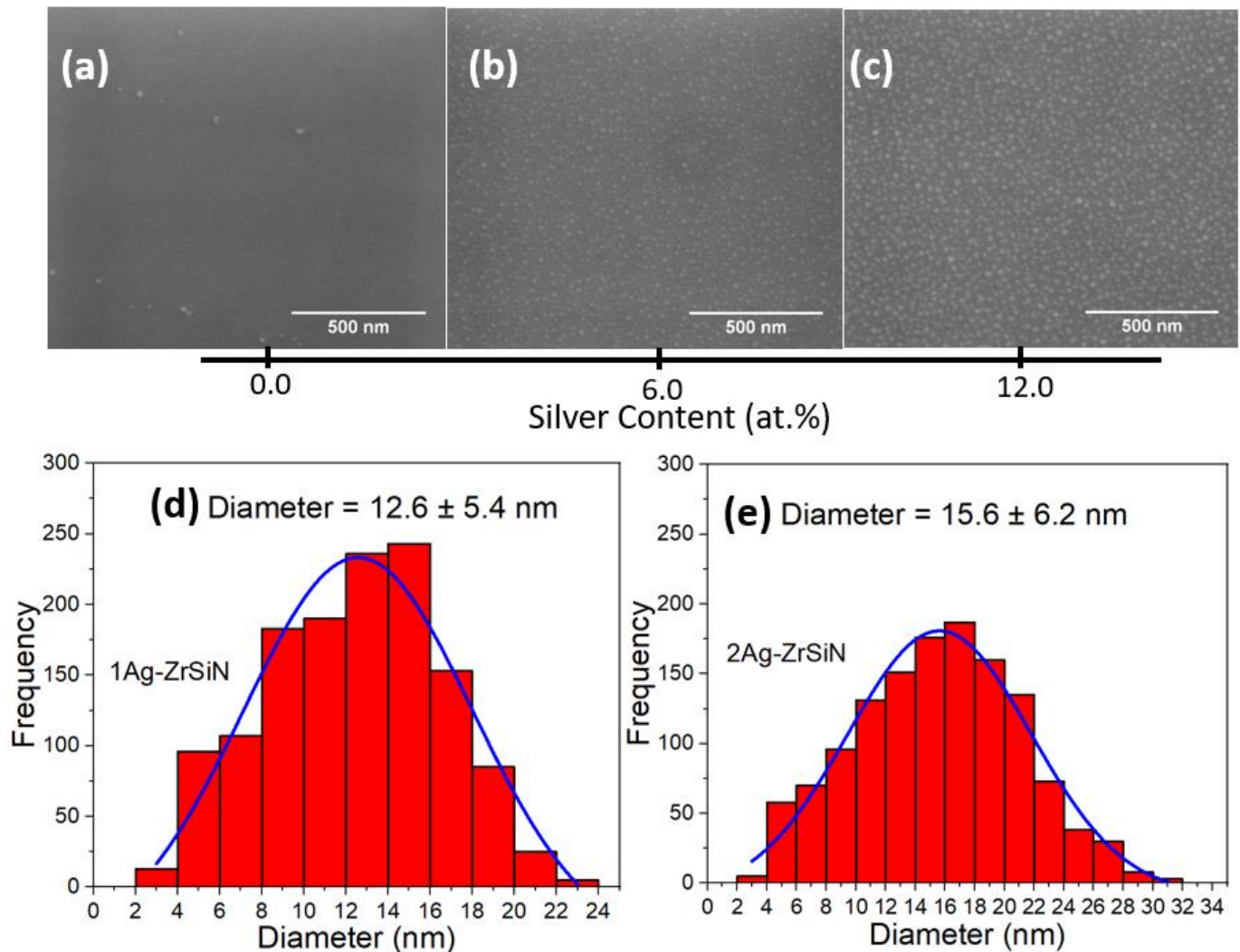


**Figure 2.** SEM images of the surface of the (a) ZrSiN, (b) 1Ag-ZrSiN, (c) 2Ag-ZrSiN coatings, and silver particle size distribution in (d) 1Ag-ZrSiN and (e) 2Ag-ZrSiN coatings.

To confirm the findings about the chemical composition of the particles observed in the SEM images, an X-ray photoelectron spectroscopy (XPS) analysis was performed. Figure 3 shows a top-view SEM image accompanied by the XPS detailed Ag 3d spectrum obtained from the 2Ag-ZrSiN sample. Figure 3a illustrates the surface morphology of the ZrSiN coating with a silver content of 12 at.%. The Ag 3d spectrum displays two prominent peaks, centered at 367.8 and 373.8 eV. These peaks correspond to Ag 3d<sub>5/2</sub> and Ag 3d<sub>3/2</sub>, respectively, with a reported separation of 6 eV between them. The peak centered at 367.8 eV exhibits two contributions, situated at positions 368.3 eV and 369.3 eV, respectively. The peak at 368.3 eV is characteristic of the formation of metallic silver, while the peak at 369.3 eV indicates the presence of small agglomerations of silver metal clusters. These results are consistent with previous investigations reported in the literature for various TiSiN-Ag [5,34,46] and ZrN-Ag [47] systems.

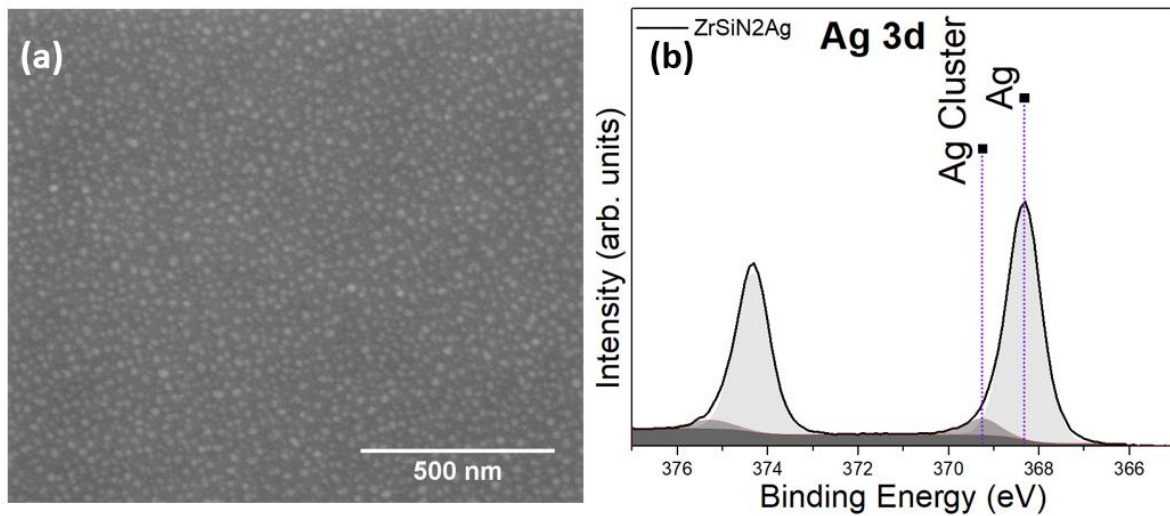


**Figure 3.** (a) Top-view SEM micrographs of the 2Ag-ZrSiN coating and (b) detailed spectrum of the Ag 3d of the surface coating.

To examine the distribution of Ag within the coating, STEM-EDS analysis was performed in order to obtain elemental mapping. Figure 4a shows a cross-sectional STEM image along with EDS line profiles of Zr, N, Si, and Ag for the Ag-ZrSiN coating with a 12 at.% Ag atomic content. The result obtained showed a homogeneous distribution of zirconium, nitrogen, silicon, and oxygen elements within the sample. However, it was observed that the distribution of silver was non-uniform throughout the coating. To investigate in detail the presence of Ag in the coating, energy-dispersive X-ray spectroscopy (EDS) mapping was carried out at a magnification of 550 kX, as depicted in Figure 4b–e. Notably, Figure 4e clearly illustrates the agglomeration of silver, resulting in the formation of nanocolumns or needle-like features. These findings strongly suggest that silver segregates to the intercolumnar space between the ZrN/SiN<sub>x</sub> columns, most likely due to the immiscibility of the Ag, SiN<sub>x</sub>, and ZrN phases.

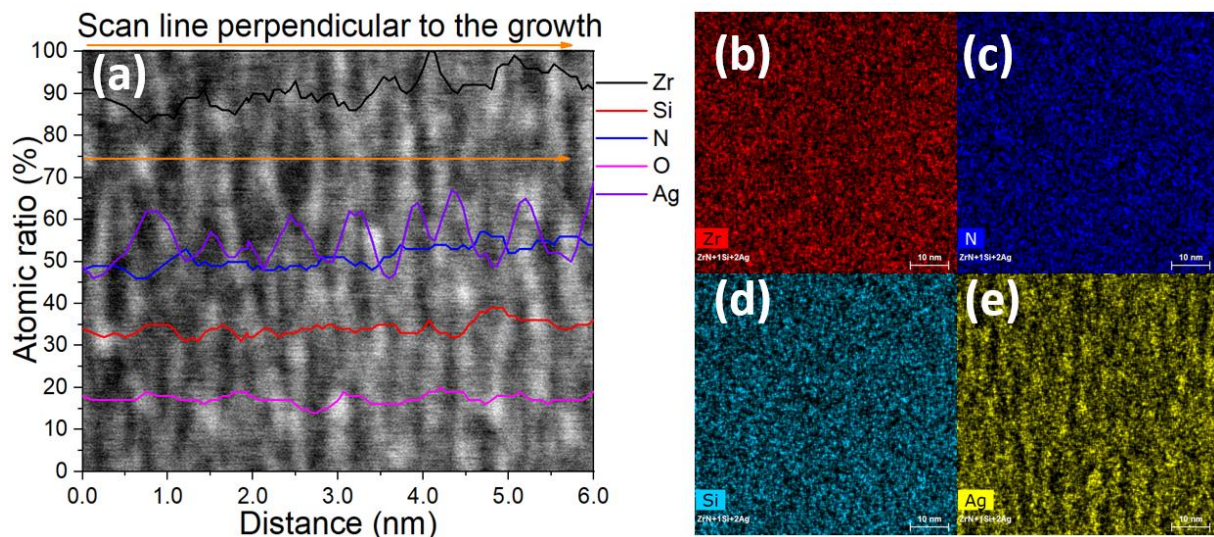


**Figure 4.** Cross-sectional image by (a) STEM and EDX elemental concentration profiles in perpendicular to the growth direction of the 2Ag-ZrSiN coating and an EDX element mapping of the coating: (b) zirconium, (c) nitrogen, (d) silicon, and (e) silver.

To investigate the formation of nanocrystalline phases in the Ag-ZrSiN coatings, X-ray diffraction (XRD) measurements were performed. Figure 5 shows the XRD patterns

of ZrSiN, 1Ag-ZrSiN, and 2Ag-ZrSiN coatings on common glass substrates. The results indicate that the ZrSiN coating exhibits wide and low-intensity diffraction peaks at approximately  $32.2^\circ$  and  $39.3^\circ$ , corresponding to an fcc-ZrN structure, as reported in the PDF (Powder Diffraction File) database (01-078-1420). No diffraction peaks associated with the crystalline phase of  $\text{Si}_3\text{N}_4$  were observed. Previous studies of ZrSiN coatings deposited under similar conditions have reported the presence of amorphous  $\text{SiN}_x$  [24]. These results suggest that the ZrSiN coating consists of a mixture of phases: a nanocrystalline fcc-ZrN and an amorphous  $\text{SiN}_x$  phase.

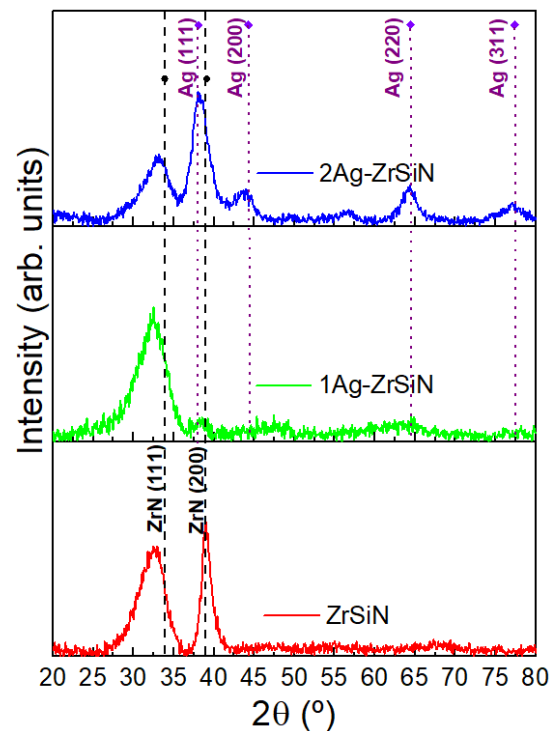


**Figure 5.** XRD patterns of Ag-ZrSiN coatings deposited on common glass substrates.

Upon incorporating Ag into the ZrSiN matrix, as observed in the 6 at.% 1Ag-ZrSiN coating, the XRD pattern does not clearly exhibit Ag-related peaks. This can be attributed to the low atomic content of Ag or to the small grain size of the Ag crystals, according to [16,43]. However, the addition of Ag results in a reduction in the intensity and a broadening of the diffraction peak associated with the ZrN (111) plane, suggesting a decrease in the grain size of ZrN crystallites and the formation of a nanocrystalline structure. As the silver content increases (12 at.%), new wide diffraction peaks with low intensity become evident at approximately around  $38.1^\circ$ ,  $44.3^\circ$ ,  $64.4^\circ$ , and  $77.4^\circ$ . These peaks are associated with the formation of metallic silver with an fcc structure, in accordance with the PDF database (01-087-0597). Nevertheless, the intensity of the ZrN (111) plane diffraction peak further decreases, suggesting that the incorporation of Ag enhances the number of nucleation sites, thereby impeding the growth of the ZrN crystals and promoting the development of a nanostructured coating. Similar results were also reported in references [5,43,48]. For instance, Cavaleiro et al. [5] observed that the incorporation of Ag leads to structural changes in the TiSiN coating. Specifically, they reported a change in the preferential orientation of the coating from (200) to (111), along with a significant broadening of TiN diffraction peaks indicative of a decrease in grain size, suggesting the formation of a nanocrystalline structure. Furthermore, they reported the presence of the white spots on surface morphology of the coating with silver. Similarly, Yu et al. [48] investigated VCN-Ag coatings with different Ag content using a magnetron sputtering system. They noted that the XRD pattern did not exhibit peaks related to the Ag phase in the range of 0 at.% to 3.69 at.% Ag. This absence of Ag peaks was attributed to the low Ag content, which did not

reach the threshold values of XRD detection. Ju et al. [43] conducted a sputtering deposition of TiN-Ag coatings and observed a reduction in the grain size of the TiN-Ag with increasing Ag content. Specifically, they found that the grain size decreased from 35 nm at 0 at.% Ag to 7 nm at 41.1 at.%.

To study the effect of Ag incorporation into the ZrSiN matrix on its functional properties, measurements of the nanohardness, optical transmittance, optical reflectance, and electrical resistivity were performed on the coatings.

### 3.3. Nanohardness of the Ag-ZrSiN Coatings

The nanohardness test results for the deposited coatings, varying the Ag content, are summarized in Table 4. The ZrSiN coating exhibited a nanohardness (H) value of approximately 18.1 GPa, which is similar to that reported for ZrN coatings [22,42,49]. When 6 at.% of Ag was incorporated, the H values remained nearly the same as those of the ZrSiN coating. This observation can be attributed to the formation of silver nanoclusters, which have a minimal impact on the nanohardness of the coating. However, with an increase in Ag content to 12 at.%, the H values decreased. This decrease can be attributed to the significant incorporation of a soft Ag phase within the coating [5,34,50], since Ag possesses a remarkably low nanohardness of 0.5 GPa [34]. Nevertheless, it is important to note that the range of nanohardness values observed for the Ag-ZrSiN coatings falls within the margin of error, suggesting that there is no statistically significant difference. However, various studies have reported that a higher concentration of soft silver within different coatings can lead to a softening effect [13,34,51].

**Table 4.** Nanohardness values and electrical resistivity of the ZrSiN, 1Ag-ZrSiN1Ag, and 2Ag-ZrSiN coatings at room temperature.

Coatings	Ag (at.%)	Nanohardness (GPa)	Resistivity ( $\Omega$ -cm)
ZrSiN	0	18.1 $\pm$ 1.6	77.99
1Ag-ZrSiN	6	17.8 $\pm$ 2.0	6.72
2Ag-ZrSiN	12	16.1 $\pm$ 2.1	0.71

### 3.4. Optical Response of the Ag-ZrSiN Coatings

The optical transmittance and the reflectance spectra of the coatings are depicted in Figure 6. The results demonstrate a reduction in the transmittance values as the Ag content increases. Additionally, an interference-like behavior can be seen in the case of the ZrSiN coating, which is a characteristic feature of semi-transparent coatings [4,52]. However, the transmittance values differ from those reported for ZrN coatings, due to the presence of the SiN<sub>x</sub> amorphous phase and ZrN nanocrystallites smaller than 10 nm, as elaborated in detail in reference [24] regarding the microstructure of these coatings. Various studies have established that SiN<sub>x</sub> coatings exhibit optical transparency in the visible to near-infrared regions [32]. In the 1Ag-ZrSiN coating, the transmittance values decrease gradually from 2500 to 630 nm and then stabilize at approximately 13.7%. By contrast, the transmittance values of the 2Ag-ZrSiN coating continue to decrease, reaching nearly zero from 630 to 300 nm, indicating an opaque behavior within that range. Different authors have reported that the Ag nanoparticles present on the surface of the coatings can exhibit light absorption in the visible and infrared wavelengths, depending on the nanoparticles' sizes and shapes [4,53]. For example, R.P. Domingues et al. [4] attributed the spectra flattening to the excitation of surface plasmons of metal nanoparticles and their respective absorption resonances. Similarly, S. Das et al. [53] reported that the low transmittance values in the visible spectrum are due to light absorption through electronic transitions. Thus, as the silver content increases, the probability of inter-band electronic excitation increases, and hence the transmittance values decrease. On the other hand, the reflectance spectra do not show an increase in reflectance values with increasing Ag content.

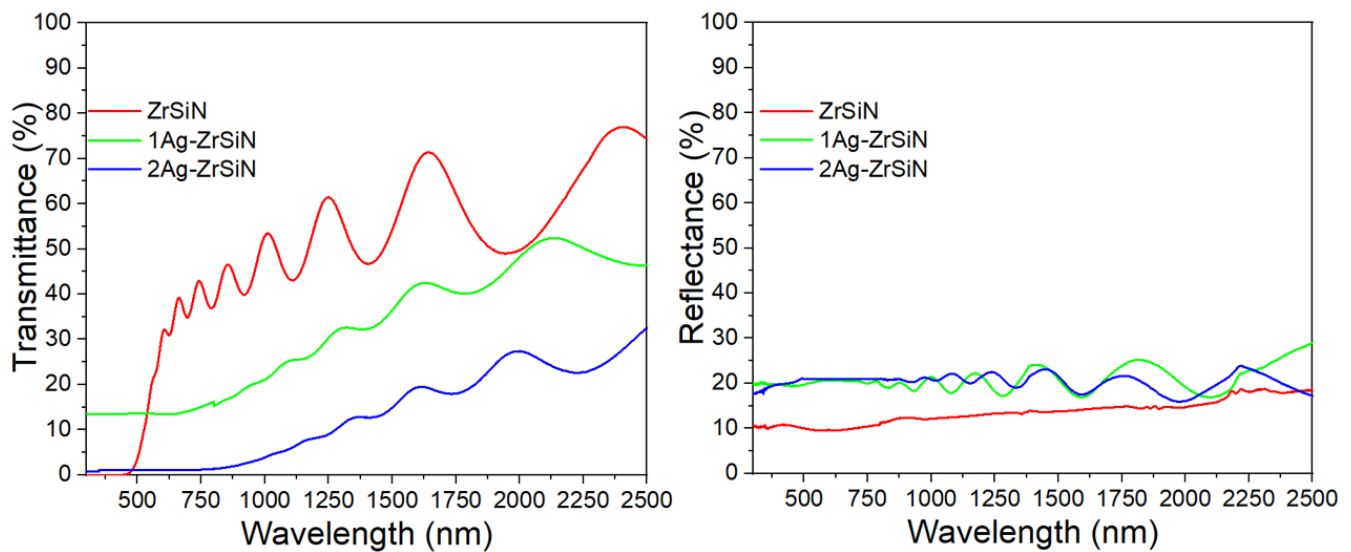


**Figure 6.** Optical transmittance and reflectance spectra of ZrSiN, 1Ag-ZrSiN, and 2Ag-ZrSiN coatings.

To determine the optical bandgap ( $E_g$ ) of the Ag-ZrSiN coatings, Tauc's relation was employed [53–56]:  $(\alpha h\nu)^n \propto h\nu - E_g$ , where  $h\nu$  represents photon energy and  $\alpha$  denotes the absorption coefficient. The  $\alpha$  values for the coatings deposited were calculated using equation [56]:  $\alpha = \frac{1}{d} \ln \frac{(1-R)^2}{T}$ , where  $d$  stands for the thickness of the coating,  $T$  represents the transmittance, and  $R$  corresponds to the reflectance. Figure 7 illustrates the Tauc's plot, where extrapolating the linear region ( $\alpha = 0$ ) provides the value of  $E_g$ . The obtained values are 1.97 eV for the ZrSiN coating and 1.20 eV and 0.87 eV for the 1Ag-ZrSiN and 2Ag-ZrSiN coatings, respectively. As can be seen, the optical bandgap decreases with an increase in the Ag content. This decrease could be attributed to the increase in carrier concentration [57], or it may be associated with the size of the silver crystallites, as evidenced by the XRD results.

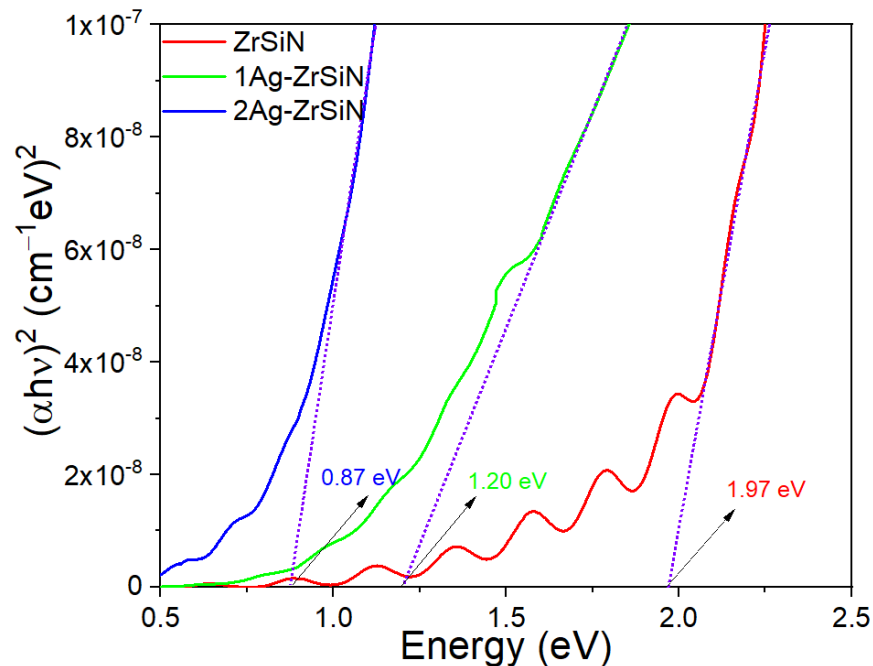


**Figure 7.** Tauc's plot for estimating the optical bandgap of ZrSiN and Ag-doped ZrSiN coatings. In our case,  $n = 2$ , due to its giving an excellent linear fit curve in the band-edge region.

### 3.5. Electrical Response of the Ag-ZrSiN Coatings

The electrical resistivity of the Ag-ZrSiN coatings was determined, and the results are presented in Table 4. The addition of silicon (Si) to the ZrSiN coating resulted in a resistivity of 77.99  $\Omega\cdot\text{cm}$ , which is higher than that reported for the ZrN coating. This effect on the electric behavior of the ZrN coatings with Si addition has been previously reported by other authors [26,58], and was attributed to the presence of the SiN<sub>x</sub> amorphous phase. With the incorporation of silver (Ag) into the ZrSiN coatings, the electrical resistivity values decreased as the Ag content increased. The 1Ag-ZrSiN coating exhibited a resistivity value of 6.72  $\Omega\cdot\text{cm}$ , while the 2Ag-ZrSiN coating had a resistivity of 0.71  $\Omega\cdot\text{cm}$ . It has been reported in the literature that the incorporation of Ag into transition-metal nitride coatings leads to a phenomenon of direct percolation between the silver nanoparticles, which are segregated into the grain boundaries of the ZrN or Zr(Si)N or into the amorphous matrix of Si<sub>3</sub>N<sub>4</sub>. Consequently, Ag incorporation into the ZrSiN matrix results in a decrease in the grain boundary effect for the SiN<sub>x</sub> matrix, leading to a decrease in the electrical resistivity values. These results are consistent with those reported by other authors [57,59]. For instance, P. Pedrosa et al. [59] deposited TiN-Ag coatings and observed changes in the electrical resistivity with varying silver content. At low silver contents, the resistivity increased, due to the presence of Ag as an impurity. However, at intermediate silver values, the resistivity decreased from  $2.25 \times 10^{-5}$  to  $5.2 \times 10^{-7}$   $\Omega\cdot\text{m}$ , and at very high silver content, the electrical resistivity of the coatings became similar to that of bulk silver ( $4 \times 10^{-7}$   $\Omega\cdot\text{m}$ ).

## 4. Conclusions

A novel nanostructured ZrSiN-Ag coating with different silver contents was deposited by means of pulsed-DC reactive magnetron sputtering. The results showed that the addition of Ag into the ZrSiN matrix induced significant changes in its morphology through the out-diffusion process of the Ag nanoparticles on surface of the coatings. Analysis of the cross-sectional STEM-EDS images confirmed the agglomeration of silver in the intercolumnar space between the ZrN/SiN<sub>x</sub> columns. Furthermore, the microstructure characterization demonstrated the formation of a nanocomposite structure, specifically nc-Ag/nc-ZrN/a-SiN<sub>x</sub>.

The electrical and optical measurements conducted exhibited the notable influence of Ag incorporation on electrical and optical behavior of the coatings. With an increase in Ag content, both the electrical resistivity and optical transmittance, along with the optical band-gap values, exhibited a decreasing trend. This behavior can be primarily attributed to the atomic content of Ag within the coatings. These findings highlight the potential to alter the electrical and optical properties of Ag-ZrSiN coatings through the incorporation of silver into the ZrSiN matrix. Such tunability presents a significant advantage, allowing for the adjustment of semi-transparency and the optical band gap by independently controlling the Ag concentration, irrespective of other parameters. This capability positions these coatings as promising candidates for optoelectronic applications.

**Author Contributions:** Conceptualization, H.S.V.P., S.C.V. and J.E.A.O.; investigation, H.S.V.P.; methodology, H.S.V.P., S.C.V. and J.J.O.F.; resources, J.J.O.F. and S.C.; writing—original draft, H.S.V.P.; writing—review and editing, H.S.V.P., S.C.V., J.E.A.O., J.J.O.F. and S.C. All authors have read and agreed to the published version of the manuscript.

**Funding:** The authors are sincerely grateful to the Universidad Antonio Nariño for its financial support of the project: “Resistencia a la corrosión del ZrN-Ag mediante impedancia electroquímica” (cod. 2020015).

**Institutional Review Board Statement:** Not applicable.

**Informed Consent Statement:** Not applicable.

**Data Availability Statement:** Not applicable.

**Acknowledgments:** This investigation was also supported by the Portuguese Foundation for Science and Technology (FCT) within the framework of the Strategic Funding (co-financed via UIDB/00285/2020) and LA/P/0112/2020.

**Conflicts of Interest:** The authors declare no conflict of interest.

## References

1. Valour, A.; Higuaita, M.A.U.; Guillonneau, G.; Crespo-Monteiro, N.; Jamon, D.; Hochedel, M.; Michalon, J.Y.; Reynaud, S.; Vocanson, F.; Jiménez, C.; et al. Optical, Electrical and Mechanical Properties of TiN Thin Film Obtained from a TiO<sub>2</sub> Sol-Gel Coating and Rapid Thermal Nitridation. *Surf. Coat. Technol.* **2021**, *413*, 127089. [[CrossRef](#)]
2. Kuznetsova, T.; Lapitskaya, V.; Khabarava, A.; Chizhik, S.; Warcholinski, B.; Gilewicz, A. The Influence of Nitrogen on the Morphology of ZrN Coatings Deposited by Magnetron Sputtering. *Appl. Surf. Sci.* **2020**, *522*, 146508. [[CrossRef](#)]
3. Gharavi, M.A.; Greczynski, G.; Eriksson, F.; Lu, J.; Balke, B.; Fournier, D.; Le Febvrier, A.; Pallier, C.; Eklund, P. Synthesis and Characterization of Single-Phase Epitaxial Cr<sub>2</sub>N Thin Films by Reactive Magnetron Sputtering. *J. Mater. Sci.* **2019**, *54*, 1434–1442. [[CrossRef](#)]
4. Domingues, R.P.; Rodrigues, M.S.; Lopes, C.; Pedrosa, P.; Alves, E.; Barradas, N.P.; Borges, J.; Vaz, F. Thin Films Composed of Metal Nanoparticles (Au, Ag, Cu) Dispersed in AlN: The Influence of Composition and Thermal Annealing on the Structure and Plasmonic Response. *Thin Solid Films* **2019**, *676*, 12–25. [[CrossRef](#)]
5. Cavaleiro, D.; Carvalho, S.; Cavaleiro, A.; Fernandes, F. TiSiN(Ag) Films Deposited by HiPIMS Working in DOMS Mode: Effect of Ag Content on Structure, Mechanical Properties and Thermal Stability. *Appl. Surf. Sci.* **2019**, *478*, 426–434. [[CrossRef](#)]
6. Borja-Goyeneche, E.N.; Olaya-Florez, J.J. A Microstructural and Corrosion Resistance Study of (Zr, Si, Ti)N-Ni Coatings Produced through Co-Sputtering. *Dyna* **2018**, *85*, 192–207. [[CrossRef](#)]
7. Chang, L.-C.C.; Zheng, Y.-Z.Z.; Chen, Y.-I.I.; Chang, S.-C.C.; Liu, B.-W.W. Bonding Characteristics and Chemical Inertness of Zr-Si-N Coatings with a High Si Content in Glass Molding. *Coatings* **2018**, *8*, 181. [[CrossRef](#)]
8. Bai, X.; Li, J.; Zhu, L.; Wang, L. Effect of Cu Content on Microstructure, Mechanical and Anti-Fouling Properties of TiSiN-Cu Coating Deposited by Multi-Arc Ion Plating. *Appl. Surf. Sci.* **2018**, *427*, 444–451. [[CrossRef](#)]
9. Shirvani, F.; Shokri, A.; Ravan, B.A. An Ab-Initio Study of Structure and Mechanical Properties of Rocksalt ZrN and Its Bilayers. *Solid State Commun.* **2021**, *328*, 114218. [[CrossRef](#)]
10. Rao, Z.; Chason, E. Measurements and Modeling of Residual Stress in Sputtered TiN and ZrN: Dependence on Growth Rate and Pressure. *Surf. Coatings Technol.* **2020**, *404*, 126462. [[CrossRef](#)]
11. Ferreira, C.P.; das Mercês Reis de Castro, M.; Tentardini, E.K.; de Freitas Cunha Lins, V.; Saliba, P.A. Silicon Influence on Corrosion Resistance of Magnetron Sputtered ZrN and ZrSiN Thin Films. *Surf. Eng.* **2020**, *36*, 33–40. [[CrossRef](#)]
12. Kumar, D.D.; Rani, R.; Kumar, N.; Panda, K.; Kirubakaran, A.M.K.; Kuppasami, P.; Baskaran, R. Tribochemistry of TaN, TiAlN and TaAlN Coatings under Ambient Atmosphere and High-Vacuum Sliding Conditions. *Appl. Surf. Sci.* **2020**, *499*, 143989. [[CrossRef](#)]
13. Mejía, H.D.; Perea, D.; Bejarano, G. Development and Characterization of TiAlN (Ag, Cu) Nanocomposite Coatings Deposited by DC Magnetron Sputtering for Tribological Applications. *Surf. Coat. Technol.* **2020**, *381*, 125095. [[CrossRef](#)]
14. Greczynski, G.; Bakhit, B.; Hultman, L.; Odén, M. High Si Content TiSiN Films with Superior Oxidation Resistance. *Surf. Coat. Technol.* **2020**, *398*, 126087. [[CrossRef](#)]
15. Cavaleiro, D.; Veeregowda, D.; Cavaleiro, A.; Carvalho, S.; Fernandes, F. High Temperature Tribological Behaviour of TiSiN(Ag) Films Deposited by HiPIMS in DOMS Mode. *Surf. Coat. Technol.* **2020**, *399*, 126176. [[CrossRef](#)]
16. AL-Rjoub, A.; Cavaleiro, A.; Fernandes, F. Influence of Ag Alloying on the Morphology, Structure, Mechanical Properties, Thermal Stability and Oxidation Resistance of Multilayered TiSiN/Ti(Ag)N Films. *Mater. Des.* **2020**, *192*, 108703. [[CrossRef](#)]
17. Ding, J.C.; Wang, Q.M.; Liu, Z.R.; Jeong, S.; Zhang, T.F.; Kim, K.H. Influence of Bias Voltage on the Microstructure, Mechanical and Corrosion Properties of AlSiN Films Deposited by HiPIMS Technique. *J. Alloys Compd.* **2019**, *772*, 112–121. [[CrossRef](#)]
18. Qiu, L.; Du, Y.; Wang, S.; Li, K.; Yin, L.; Wu, L.; Zhong, Z.; Albir, L. Mechanical Properties and Oxidation Resistance of Chemically Vapor Deposited TiSiN Nanocomposite Coating with Thermodynamically Designed Compositions. *Int. J. Refract. Met. Hard Mater.* **2019**, *80*, 30–39. [[CrossRef](#)]
19. Warcholinski, B.; Kuznetsova, T.A.A.; Gilewicz, A.; Zubar, T.I.I.; Lapitskaya, V.A.A.; Chizhik, S.A.A.; Komarov, A.I.I.; Komarova, V.I.I.; Kuprin, A.S.S.; Ovcharenko, V.D.D.; et al. Structural and Mechanical Properties of Zr-Si-N Coatings Deposited by Arc Evaporation at Different Substrate Bias Voltages. *J. Mater. Eng. Perform.* **2018**, *27*, 3940–3950. [[CrossRef](#)]
20. Gao, Z.; Chen, Y.; Kulczyk-malecka, J.; Kelly, P.; Zeng, Y.; Zhang, X. Comparison of the Oxidation Behavior of a Zirconium Nitride Coating in Water Vapor and Air at High Temperature. *Corros. Sci.* **2018**, *138*, 242–251. [[CrossRef](#)]
21. Krysin, O.V.; Ivanov, Y.F.; Prokopenko, N.A.; Shugurov, V.V.; Petrikova, E.A.; Denisova, Y.A.; Tolkachev, O.S. Influence of Nb Addition on the Structure, Composition and Properties of Single-Layered ZrN-Based Coatings Obtained by Vacuum-Arc Deposition Method. *Surf. Coat. Technol.* **2020**, *387*, 125555. [[CrossRef](#)]
22. Silva Neto, P.C.; Freitas, F.G.R.; Fernandez, D.A.R.; Carvalho, R.G.; Felix, L.C.; Terto, A.R.; Hubler, R.; Mendes, F.M.T.; Silva Junior, A.H.; Tentardini, E.K. Investigation of Microstructure and Properties of Magnetron Sputtered Zr-Si-N Thin Films with Different Si Content. *Surf. Coat. Technol.* **2018**, *353*, 355–363. [[CrossRef](#)]

23. Mejía, C.P.; Chellali, M.R.; Garzón, C.M.; Olaya, J.J.; Hahn, H.; Velasco, L. Effect of Discharge Current on the Corrosion Resistance and Microstructure of ZrTiSiN Coatings Deposited by Magnetron Co-Sputtering. *Mater. Today Commun.* **2021**, *26*, 102151. [[CrossRef](#)]
24. Vanegas P, H.S.; Calderon V, S.; Alfonso O, J.E.; Olaya F, J.J.; Ferreira, P.J.; Carvalho, S. Influence of Silicon on the Microstructure and the Chemical Properties of Nanostructured ZrN-Si Coatings Deposited by Means of Pulsed-DC Reactive Magnetron Sputtering. *Appl. Surf. Sci.* **2019**, *481*, 1249–1259. [[CrossRef](#)]
25. Cao, F.; Munroe, P.; Zhou, Z.; Xie, Z. Mechanically Robust TiAlSiN Coatings Prepared by Pulsed-DC Magnetron Sputtering System: Scratch Response and Tribological Performance. *Thin Solid Films* **2018**, *645*, 222–230. [[CrossRef](#)]
26. Ghafoor, N.; Petrov, I.; Klenov, D.O.; Freitag, B.; Jensen, J.; Greene, J.E.; Hultman, L.; Odén, M. Self-Organized Anisotropic (Zr<sub>1-x</sub>Si<sub>x</sub>)N<sub>y</sub> Nanocomposites Grown by Reactive Sputter Deposition. *Acta Mater.* **2015**, *82*, 179–189. [[CrossRef](#)]
27. Yalamanchili, K.; Forsén, R.; Jiménez-Piqué, E.; Johansson Jöesaar, M.P.; Roa, J.J.; Ghafoor, N.; Odén, M. Structure, Deformation and Fracture of Arc Evaporated Zr-Si-N Hard Films. *Surf. Coat. Technol.* **2014**, *258*, 1100–1107. [[CrossRef](#)]
28. Geng, D.; Zeng, R.; Rong, M.; Wang, Q.; Li, H.; Wu, Z. Impact of Si Addition on Oxidation Resistance of Zr–Si–N Nanocomposite Films. *Vacuum* **2021**, *183*, 109853. [[CrossRef](#)]
29. Velasco, L.; Olaya, J.J.; Rodil, S.E. Effect of Si Addition on the Structure and Corrosion Behavior of NbN Thin Films Deposited by Unbalanced Magnetron Sputtering. *Appl. Phys. A Mater. Sci. Process* **2016**, *122*, 101. [[CrossRef](#)]
30. Mishra, S.K.; Kumari, S. Soni Development of Hard and Optically Transparent Al-Si-N Nanocomposite Coatings. *Surf. Interface Anal.* **2017**, *49*, 345–348. [[CrossRef](#)]
31. Vanegas, H.S.; Alfonso, J.E.; Olaya, J.J. Effect of Si Content on Functional Behavior of Nanostructured Coatings of Zr-Si-N. *Mater. Res. Express* **2019**, *6*, 115076. [[CrossRef](#)]
32. Kulczyk-Malecka, J.; Kelly, P.J.; West, G.; Clarke, G.C.B.; Ridealgh, J.A. Diffusion Studies in Magnetron Sputter Deposited Silicon Nitride Films. *Surf. Coat. Technol.* **2014**, *255*, 37–42. [[CrossRef](#)]
33. Musil, J.; Daniel, R.; Zeman, P.; Takai, O. Structure and Properties of Magnetron Sputtered Zr-Si-N Films with a High ( $\geq 25$  at.%) Si Content. *Thin Solid Films* **2005**, *478*, 238–247. [[CrossRef](#)]
34. Dang, C.; Li, J.; Wang, Y.; Yang, Y.; Wang, Y.; Chen, J. Influence of Ag Contents on Structure and Tribological Properties of TiSiN-Ag Nanocomposite Coatings on Ti-6Al-4V. *Appl. Surf. Sci.* **2017**, *394*, 613–624. [[CrossRef](#)]
35. Popović, M.; Novaković, M.; Rakočević, Z.; Bibić, N. Tailoring the Structural and Optical Properties of TiN Thin Films by Ag Ion Implantation. *Nucl. Instrum. Methods Phys. Res. Sect. B Beam Interact. Mater. Atoms* **2016**, *389–390*, 33–39. [[CrossRef](#)]
36. Sun, H.; Billard, A.; Luo, H.; Zheng, W.T.; Zheng, X.L.; Dai, M.J.; Lin, S.S.; Shi, Q.; Sanchette, F. Influence of Carbon Content on the Mechanical Properties of TiCN–Cu Nanocomposite Coatings Prepared by Multi-Arc Ion Plating. *Vacuum* **2021**, *187*, 110139. [[CrossRef](#)]
37. Byun, M.; Kim, C.S.; Kim, D.H.; Hwang, J.U.; Lee, J.H.; Park, E.S. A 3D Printing Route to Fabrication of ZrCuSi Alloy Target for ZrCuSiN Nanocomposite Thin Films. *Appl. Surf. Sci.* **2021**, *562*, 150136. [[CrossRef](#)]
38. Luo, X.Y.; Ma, D.L.; Jing, P.P.; Gong, Y.L.; Zhang, Y.; Jing, F.J.; Leng, Y.X. In Vitro Analysis of Cell Compatibility of TiCuN Films with Different Cu Contents. *Surf. Coat. Technol.* **2021**, *408*, 126790. [[CrossRef](#)]
39. Hu, C.; Guo, K.; Li, Y.; Gu, Z.; Quan, J.; Zhang, S.; Zheng, W. Optical Coatings of Durability Based on Transition Metal Nitrides. *Thin Solid Films* **2019**, *688*, 137339. [[CrossRef](#)]
40. Cui, X.; Jin, G.; Hao, J.; Li, J.; Guo, T. The Influences of Si Content on Biocompatibility and Corrosion Resistance of Zr-Si-N Films. *Surf. Coat. Technol.* **2013**, *228*, 524–528. [[CrossRef](#)]
41. Brandes, E. *Smithells Metals Reference Book*, 7th ed.; Brandes, E., Brook, G., Eds.; Butterworth: London, UK, 1983; ISBN 0750636246.
42. Ju, H.; Yu, D.; Yu, L.; Ding, N.; Xu, J.; Zhang, X.; Zheng, Y.; Yang, L.; He, X. The Influence of Ag Contents on the Microstructure, Mechanical and Tribological Properties of ZrN-Ag Films. *Vacuum* **2018**, *148*, 54–61. [[CrossRef](#)]
43. Ju, H.; Yu, L.; Yu, D.; Asempah, I.; Xu, J. Microstructure, Mechanical and Tribological Properties of TiN-Ag Films Deposited by Reactive Magnetron Sputtering. *Vacuum* **2017**, *141*, 82–88. [[CrossRef](#)]
44. Rajput, S.S.; Gangopadhyay, S.; Cavaleiro, A.; AL-Rjoub, A.; Kumar, C.S.; Fernandes, F. Influence of Ag Additions on the Structure, Mechanical Properties and Oxidation Behaviour of CrAlNAg Coatings Deposited by Sputtering. *Surf. Coat. Technol.* **2021**, *426*, 127767. [[CrossRef](#)]
45. Zhu, Y.; Dong, M.; Li, J.; Wang, L. The Improved Corrosion and Tribocorrosion Properties of TiSiN/Ag by Thermal Treatment. *Surf. Coat. Technol.* **2020**, *385*, 125437. [[CrossRef](#)]
46. Dang, C.; Yao, Y.; Olugbade, T.; Li, J.; Wang, L. Effect of Multi-Interfacial Structure on Fracture Resistance of Composite TiSiN/Ag/TiSiN Multilayer Coating. *Thin Solid Films* **2018**, *653*, 107–112. [[CrossRef](#)]
47. Mejía, C.P.; Vanegas, H.S.; Olaya, J.J. Electrochemical and Optical Behavior of ZrN-Ag Coatings Deposited by Means of DC Reactive Magnetron Sputtering Technique. *Coatings* **2022**, *12*, 754. [[CrossRef](#)]
48. Yu, D.; Yu, L.; Asempah, I.; Ju, H.; Xu, J.; Koyama, S.; Gao, Y. Microstructure, Mechanical and Tribological Properties of VCN-Ag Composite Films by Reactive Magnetron Sputtering. *Surf. Coat. Technol.* **2020**, *399*, 126167. [[CrossRef](#)]
49. Chen, Y.I.; Chang, S.C.; Chang, L.C. Oxidation Resistance and Mechanical Properties of Zr–Si–N Coatings with Cyclic Gradient Concentration. *Surf. Coat. Technol.* **2017**, *320*, 168–173. [[CrossRef](#)]
50. Manninen, N.K.; Ribeiro, F.; Escudeiro, A.; Polcar, T.; Carvalho, S.; Cavaleiro, A. Influence of Ag Content on Mechanical and Tribological Behavior of DLC Coatings. *Surf. Coat. Technol.* **2013**, *232*, 440–446. [[CrossRef](#)]

51. Ren, P.; Zhang, K.; He, X.; Du, S.; Yang, X.; An, T.; Wen, M.; Zheng, W. Toughness Enhancement and Tribochemistry of the Nb-Ag-N Films Actuated by Solute Ag. *Acta Mater.* **2017**, *137*, 1–11. [[CrossRef](#)]
52. Borges, J.; Costa, D.; Antunes, E.; Lopes, C.; Rodrigues, M.S.; Apreutesei, M.; Alves, E.; Barradas, N.P.; Pedrosa, P.; Moura, C.; et al. Biological Behaviour of Thin Films Consisting of Au Nanoparticles Dispersed in a TiO<sub>2</sub> Dielectric Matrix. *Vacuum* **2015**, *122*, 360–368. [[CrossRef](#)]
53. Das, S.; Alford, T.L. Structural and Optical Properties of Ag-Doped Copper Oxide Thin Films on Polyethylene Naphthalate Substrate Prepared by Low Temperature Microwave Annealing. *J. Appl. Phys.* **2013**, *113*, 1–7. [[CrossRef](#)]
54. Jalili, S.; Hajakbari, F.; Hojabri, A. Effect of Silver Thickness on Structural, Optical and Morphological Properties of Nanocrystalline Ag/NiO Thin Films. *J. Theor. Appl. Phys.* **2018**, *12*, 15–22. [[CrossRef](#)]
55. El Rouby, W.M.A.; Al-Ghamdi, A.A.; Abdel-Wahab, M.S.; Jilani, A. Sunlight-Enhanced Catalytic Degradation over Ag-CuO Nanoparticles Thin Films Prepared by DC/RF Sputtering Technique. *Bull. Mater. Sci.* **2018**, *41*, 58. [[CrossRef](#)]
56. Zanatta, A.R. Revisiting the Optical Bandgap of Semiconductors and the Proposal of a Unified Methodology to Its Determination. *Sci. Rep.* **2019**, *9*, 11225. [[CrossRef](#)]
57. Kumar, K.S.; Manohari, A.G.; Dhanapandian, S.; Mahalingam, T. Physical Properties of Spray Pyrolyzed Ag-Doped SnS Thin Films for Opto-Electronic Applications. *Mater. Lett.* **2014**, *131*, 167–170. [[CrossRef](#)]
58. Sanjines, R.; Sandu, C.S. Interfacial Electron Scattering in Nanocomposite Materials: Electrical Measurements to Reveal the Nc-MeN/a-SiNx Nanostructure in Order to Tune Macroscopic Properties. In *Nanocomposites—New Trends and Developments*; InTech: Nappanee, IN, USA, 2012.
59. Pedrosa, P.; Machado, D.; Lopes, C.; Alves, E.; Barradas, N.P.; Martin, N.; Macedo, F.; Fonseca, C.; Vaz, F. Nanocomposite Ag:TiN Thin Films for Dry Biopotential Electrodes. *Appl. Surf. Sci.* **2013**, *285*, 40–48. [[CrossRef](#)]

**Disclaimer/Publisher's Note:** The statements, opinions and data contained in all publications are solely those of the individual author(s) and contributor(s) and not of MDPI and/or the editor(s). MDPI and/or the editor(s) disclaim responsibility for any injury to people or property resulting from any ideas, methods, instructions or products referred to in the content.